IOPscience iopscience.iop.org

Home Search Collections Journals About Contact us My IOPscience

Collapse of molecularly thin lubricant layers between elastic substrates

This article has been downloaded from IOPscience. Please scroll down to see the full text article.

2003 J. Phys.: Condens. Matter 15 S321

(http://iopscience.iop.org/0953-8984/15/1/344)

View the table of contents for this issue, or go to the journal homepage for more

Download details:
IP Address: 171.66.16.97
The article was downloaded on 18/05/2010 at 19:25

Please note that terms and conditions apply.

INSTITUTE OF PHYSICS PUBLISHING JOURNAL OF PHYSICS: CONDENSED MATTER

J. Phys.: Condens. Matter **15** (2003) S321–S330 PII: S0953-8984(03)55176-1

Collapse of molecularly thin lubricant layers between elastic substrates

T Becker and F Mugele

Department of Applied Physics, University of Ulm, Albert Einstein Allee 11, D-89069 Ulm, Germany

Received 23 October 2002
Published 16 December 2002
Online at stacks.iop.org/JPhysCM/15/S321

Abstract

We investigated the dynamics of layering transitions and other structure formation processes in molecularly thin liquid films upon reducing the separation between two atomically smooth mica substrates. Using a newly developed surface forces apparatus with two-dimensional imaging capability, we followed the hydrodynamic processes during drainage with unprecedented precision. Depending on the substrate elasticity and the approach rate, drainage occurs either in a series of consecutive layering transitions or in a single step. In the latter case, nanoscopic amounts of liquid are trapped inside the contact area transiently. The experimental observations are explained qualitatively by combining hydrodynamic effects with elastic deformations of the substrates. Furthermore, we present evidence for anisotropy in the fluid dynamics induced by the lattice symmetry of the substrates.

1. Introduction

Thin liquid films between solid substrates have attracted much attention in recent years [1–16] because of their important role in many biological, geological and technological problems. It was shown that the properties of the films can no longer be described by extrapolating the bulk properties if the thickness is in the range of a few molecular diameters. Computer hard drives and microelectromechanical systems (MEMS) are just two examples where lubricant layers in this range of film thickness are used in modern technical devices. The presence of the ultrathin lubricant layers is crucial for the operation and lifetime of these devices. If they collapse and become expelled from the gap between the two sliding surfaces, catastrophically large wear occurs and the devices fail. It is thus of utmost importance to understand the mechanisms that govern the stability of lubricant layers in this range of film thickness.

The fundamental effects of confinement and solid–liquid interaction on the structural and mechanical properties of thin liquid films can be studied most accurately in a well defined geometry with planar substrates. Such a geometry is realized in a surface forces apparatus (SFA) [2], where two atomically smooth mica surfaces confine the liquid to a gap of

 © 2003 IOP Publishing Ltd Printed in the UK

adjustable width. It was shown previously that confined liquids display a completely different behaviour from the bulk. For instance, the film thickness decreases continuously if the two substrates are pressed together as long as its properties follow the behaviour of the bulk liquid. When the film thickness is reduced to a few molecular diameters, however, the thickness decreases in a steplike fashion instead of continuous drainage. This behaviour is due to the arrangement of molecules in layers parallel to the smooth walls, as shown previously. Each step corresponds to the expulsion of a single layer of liquid molecules and was thus termed layering transition. Recent experiments [4] and theory [15–18] indicated that the elastic properties of the confining walls play an important role.

In the present contribution, we use a modified SFA [4, 5] that allows for a two-dimensional analysis of the dynamic process in molecularly thin films in order to study in detail the collapse dynamics of molecularly thin lubricant films upon increasing normal pressure. We show that completely different scenarios are obtained, depending on the substrate elasticity and on the drainage rate, i.e. the approach velocity of the substrates. We first review a few fundamental aspects of hydrodynamic drainage between hard and soft substrates. Next a short experimental section describes the key features of our setup. Then, we present and discuss our experimental results both with hard and with soft substrates, and close with a few concluding remarks.

2. Theory

Let us consider first a thick fluid layer between a rigid flat circular disc (radius R) and a rigid flat surface. If the disc is pressed towards the flat with a force F (that can be infinitely small), the thickness h ($h \ll R$) of the fluid layer decreases continuously with time. Let us assume that the velocity field of the fluid satisfies the Navier–Stokes equation for an incompressible liquid and introduce cylindrical coordinates (ρ, z, t). The velocity profile across the gap will be parabolic. If we assume no-slip boundary conditions at the solid–liquid interfaces, the surface separation $h(t)$ as a function of time is given by [1, 17, 18]

$$h(t) = \left(\frac{4tP}{3\mu R^2} + \frac{1}{h^2(0)} \right)^{-1/2}. \tag{1}$$

In this equation μ denotes the viscosity of the liquid and $P = F/(\pi R^2)$ is the pressure. However, if F is really small, the thickness of the liquid film will in general not decrease to zero and a fluid slab with thickness of a few molecular layers will remain trapped between the solid surfaces. In this range, a finite threshold force is required to reduce the film thickness from an integral multiple n of the molecular diameter to $(n - 1)$. The fact that the film withstands a finite normal stress reflects the oscillatory density profile of the fluid in this range, i.e. the layered arrangement of the molecules. If the substrates are perfectly rigid, the film thickness must decrease by one molecular diameter simultaneously over the whole contact area. Such a process would involve a large activation barrier, because it requires a density fluctuation of the liquid over a macroscopic distance. In reality, however, the substrates always have a finite elasticity. This reduces considerably the activation barrier for layering transitions. Persson and Tosatti [18] presented a model that describes the nucleation and the subsequent dynamics of layering transitions. In their model, they consider a film of thickness n, which is in a metastable state because the applied pressure exceeds the threshold pressure for this thickness. A thermal fluctuation in the film creates a small circular region with radius ρ within the film, where the liquid density is reduced. Because of the reduced density, the liquid locally can no longer balance the normal pressure exerted by the substrates. Hence the substrates can relax inward elastically within the radius ρ. This little nucleus of thickness $(n - 1)$ grows, if the energy gain due to this elastic relaxation exceeds the restoring forces that tend to close the hole

again. In the model of Persson and Tosatti [18] there are three contributions to the energy of the nucleus:

$$U(\rho) = 2\pi\rho\Gamma + \pi\rho^2 p_0 - (1-\nu^2)\frac{P_{3D}^2 c}{E}\rho^3. \tag{2}$$

The first term is the contribution of the line energy along the circumference of the nucleus with Γ representing the line tension. The second term is the change in the interface free energy with the spreading pressure p_0. In this geometry, the latter also contains a contribution from the applied normal pressure P_{3D}: $p_0(r) = P_{2D} + P_{3D}(r)h$. The last term in equation (2) represents an elastic relaxation energy of the substrate within the area of the nucleus. This contribution, in which E denotes the effective elastic modulus of the substrates, ν is the Poisson ratio and c is a numerical constant of the order of unity, stabilizes the nucleus. If ρ exceeds a critical radius $\rho_c(\approx 2$ nm), the nucleus grows. It is obvious from equation (2) that ρ_c is smaller for softer substrates. The local relaxation of the substrates reduces the potential barriers for the nucleation of layering transitions and thus destabilizes the lubricant layer. Once a sufficiently large nucleus has been generated, it spreads over the whole contact area within a short time. In the final state, the film thickness is $(n-1)$ everywhere. This subsequent growth process can be described with a two-dimensional potential flow, as suggested earlier theoretically [1, 18] and recently proven experimentally [4, 6, 17].

Besides the nucleation barrier, the substrate elasticity also affects the preferential location for the nucleation in the experiments. In the SFA geometry, the mica sheets that confine the liquid are mounted in crossed cylinder geometry, which is equivalent to a sphere in contact with a plane. Therefore, the pressure distribution across the contact area is not homogeneous as in the example just discussed, but it obeys the Hertzian formula of contact mechanics:

$$P(\rho) = \frac{3}{2}P_{ext}\left(1 - \left(\frac{\rho}{R}\right)^2\right)^{1/2}. \tag{3}$$

Since nucleation preferentially occurs where the pressure is maximum, layering transitions are expected to nucleate close to the centre of the contact area.

3. Experimental details

All the experiments were performed in a home-built SFA, which was described in detail earlier [5]. The substrates, two backside-silvered mica sheets glued on glass sheets (thickness ≈ 80 μm), which are fixed on a stainless steel sample holder (radius of curvature 5 cm), are mounted in a crossed cylinder configuration and form a Fabry–Pérot interferometer. In contrast to the conventional setup, we illuminated the sample with monochromatic light. The wavelength was adjusted to one side of one of the transmission peaks of the interferometer (figure 1). Two-dimensional images of the contact region were recorded with a video microscope.

In order to vary the effective elasticity of the substrates, we used mica sheets of different thicknesses ranging from approximately 0.4–1.5 μm. The thinner the mica sheets, the smaller the effective elastic modulus, because the underlying polymeric glue layer contributes more. Mica sheets in this range of thickness were obtained by recleaving the conventionally prepared SFA substrates with sticky tape after they were mounted on the cylindrical holders [4, 6, 19]. In addition to allowing for the preparation of very thin mica sheets, this procedure also leads to particularly clean mica substrates. In particular, nano-particles that are generated during the conventional preparation procedure, which may disturb the measurements, are removed by this procedure [6, 20].

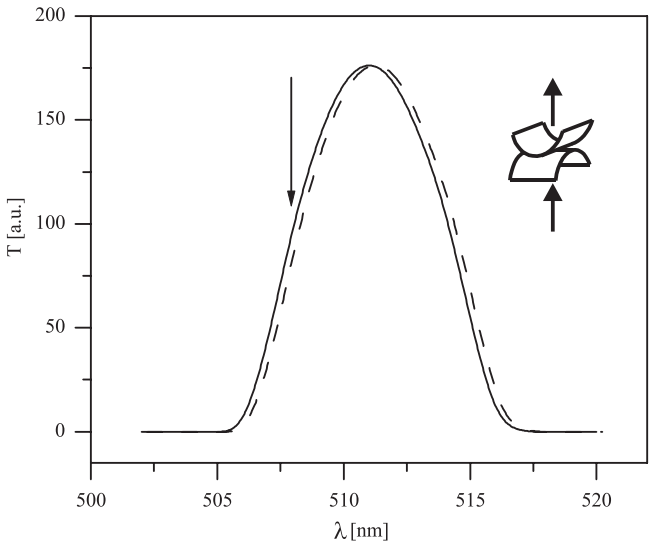

Figure 1. Transmitted intensity $T(\lambda)$ averaged over an area of $10 \times 10\ \mu\text{m}^2$ within the contact area (dry contact) (solid curve). After injecting the liquid, the mirrors are further apart and the peak is shifted to a larger wavelength (dashed curve). The arrow indicates the wavelength λ at which the images in figure 3 were recorded. The inset shows schematically the experimental setup.

After the recleavage, the combined thickness of the two mica sheets was measured. The substrates were brought into contact in dry air atmosphere, and we recorded the average intensity transmitted in the centre of the contact area as a function of wavelength λ between 450 and 650 nm. From these data, we calculated the thickness of the mica sheets easily using the matrix method for optical multilayer interference [5, 21]. Figure 1 shows a detail with just one transmission peak.

The experiments were performed with octamethylcyclotetrasiloxane (OMCTS, obtained from ABCR, Karlsruhe, Germany; water content 3 ppm), a non-polar liquid with quasi-spherical molecules (diameter 0.9 nm). Droplets of $\approx 10\ \mu$l were deposited between the mica surfaces with a syringe. After that, the substrates were equilibrated at a separation of a few micrometres. Subsequently, the upper surface was pressed against the lower one with a normal force that was increased continuously from zero to 15 mN. Video images were recorded at equidistant time intervals while increasing the load. The experiments were performed at room temperature $22 \pm 1\,^{\circ}$C.

4. Results and discussion

4.1. Thick mica

In the first type of experiment that we describe here, the combined thickness of the mica sheets was 2.5 μm. The transmission peak shown in figure 1 was obtained with this set of mica surfaces. We adjusted the wavelength to the left edge of the transmission peak. In this case, the transmitted intensity increases if the thickness of the liquid layer decreases. Upon increasing the load the substrates approached a separation of a few nanometres and flattened elastically. At the highest load the contact zone had a diameter of $\approx 65\ \mu$m. In figure 2, we plot the transmitted intensity (averaged over an area of $10 \times 10\ \mu\text{m}^2$) as a function of time. The zero

of time is arbitrary. It corresponds to a film thickness of approximately 20 nm. One can clearly see that the value of h initially decreases continuously, but later on displays a series of three discrete steps with plateaus in between. Using $T(\lambda)$ from figure 1 we calibrated the intensity steps. Each step was found to correspond to a reduction in film thickness of 0.95 ± 0.1 nm. This is in good agreement with the diameter of 0.9 nm of the OMCTS molecules, as found in recent studies [7, 9–14]. Under the conditions of the present experiment, the value of h thus decreases in a series of discrete layering transitions, as expected. However, our two-dimensional imaging techniques allow for a much more detailed analysis of the transition from thickness n to $(n-1)$. Figure 3 shows snapshots during the $n = 3 \rightarrow 2$ transition from the recorded video (around $t = 15$ s in figure 2). In the first image the metastable $n = 3$ layer is still homogeneous. In the next image a bright area appears close to the centre of the contact area. Here, the thickness is locally reduced to $n = 2$. In the following the $n = 2$ area spreads over the whole contact area within 3 s as the metastable layer is expelled. For transitions with larger n the collapse dynamics are qualitatively the same. However, fewer images could be recorded due to the shorter time for the layer expulsion in that case. The scenario was found to be independent of the loading rate within the range investigated here. Nucleation was always detected close to the centre, as expected from equations (2) and (3). In total, we could follow four layering transitions from $n = 5$ down to $n = 2$ at different contact positions [6]. We analysed the velocity of the boundary lines between the n and the $(n-1)$ areas and found good agreement with the hydrodynamic model developed by Persson and Tosatti [17, 18]. Furthermore, we determined the frictional coefficient η, which characterizes the dissipation during the expulsion of the liquid layers. It was found to increase only weakly with decreasing film thickness. The friction for the $2 \rightarrow 1$ transition was found to be only one order of magnitude larger than for the $5 \rightarrow 4$ transition. This is a very surprising result because earlier experiments suggested that the friction in molecularly thin liquid films increases by several orders of magnitude with respect to the bulk [11–14]. As we discussed elsewhere [6], this discrepancy is probably related to contamination problems in the earlier experiments, which result from the surface preparation procedure [20].

In addition to the qualitative behaviour discussed so far, figure 3 reveals more interesting details on the boundary line dynamics: a close inspection of the images shows that the bright $(n-1)$ areas are not round, as one would expect on theoretical grounds. Rather they have a tendency to display edges and facets. Adjacent edges seem to cross at angles of approximately 60°, as indicated by the dashed white lines in the sixth image in figure 3. In order to analyse the tendency in detail, we extracted the boundary lines from the images. Then we determined the orientation of short segments between adjacent pixels of the boundary line along the circumference of the island. In figure 4, we show a histogram of the segment orientations of the boundary taken from the sixth image in figure 3. Similar histograms were obtained for several other images, too. The histograms indicate that there is indeed a preferred angle of 60° between adjacent facets of the boundary line. This is reminiscent of the pseudo-hexagonal structure of the mica substrate. In fact, recent Monte Carlo simulations of OMCTS layers confined between mica surfaces [22] showed that the OMCTS molecules adopt a quasi-hexagonal structure. Similar effects were seen in recent x-ray diffraction experiments, where a Si(100) surface was shown to affect the structure in an adjacent liquid lead [23]. It is reasonable to assume that this structure of the layers also affects the transport properties, which determine the dynamics in our experiments. If the diffusion coefficient of the molecules or the friction coefficient η in the hydrodynamic model by Persson and Tossati [17, 18] is anisotropic, this should lead to the observed faceting. We note, however, that this result is not routinely reproduced in consecutive experiments. Most likely, the effect is very sensitive to the alignment of the lattice in the two opposing mica sheets. Currently, we can only control this

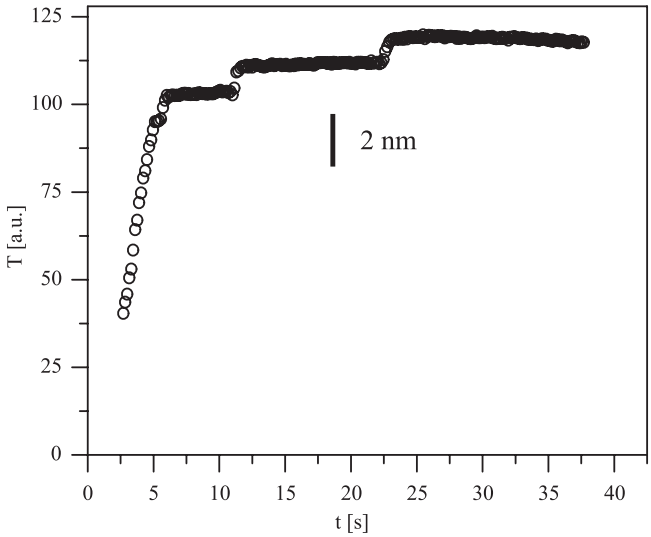

Figure 2. Transmitted intensity (array of 10×10 μm^2 in the centre of the contact area) versus time ($d_{Mica,total} = 2.5$ μm). Three discrete steps can be seen between which the intensity remains nearly constant.

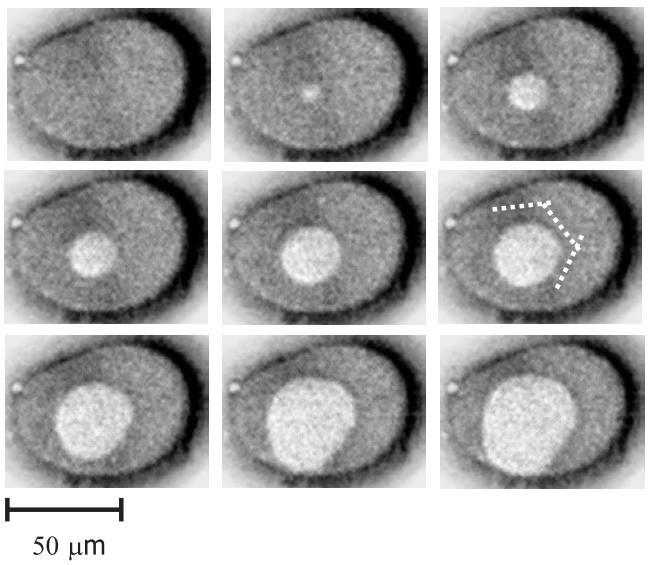

Figure 3. Snapshots from the last layering transition from figure 2. In the second image a bright area, corresponding to a reduced liquid film thickness, appears in the centre of the contact region and spreads afterwards. The time difference between the images is 0.15 s. The angle between the dashed lines is 60°.

alignment to within approximately ±5°. A detailed investigation of epitaxial effects requires better control and precise variation of the mutual alignment, which cannot be achieved without substantial modifications of the experimental setup.

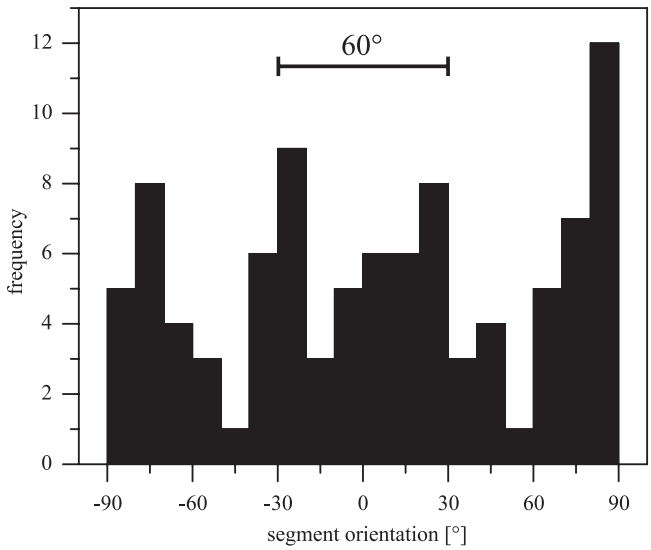

Figure 4. In the experiment with thick substrates some straight segments in the boundary line can be seen. This histogram represents the line orientation. Obviously, some orientations are preferred.

4.2. Thin mica

In a second set of experiments, we used much thinner mica substrates with a total thickness of 820 nm. In this case, the collapse dynamics was found to depend strongly on the loading rate. For loading rates less than a certain critical value (4 mN s^{-1} for the data presented here), the lubricant collapse was similar to the scenario described above, except that we could detect only one single layering transition. Tentatively, we attribute the absence of the transitions at higher n to the reduction of the activation barriers for soft substrates. This prevents the observation of the transitions.

If the loading rate is increased above the critical value, the scenario changes completely. Figure 5 shows a series of snapshots recorded after a stepwise increase of the load from 0 to 15 mN. Under these conditions, the nucleation of the $(n - 1)$ area occurs at several positions along the edge of the contact zone within a rather short time (first and second rows in figure 5). (In this experiment, the wavelength of the illuminating light was adjusted to the right side of the transmission peak. Therefore, darker grey levels correspond to thinner films in this figure.) The nuclei grow while more and more nuclei continue to appear. Some material from the monolayer is expelled from the contact area, while the rest accumulates in a single patch close to the centre of the contact area. This patch shrinks laterally with time and eventually transforms into an approximately circular droplet (see the inset of figure 6(b)), which is brighter, i.e. thicker, than the initial film. Remarkably, a cross-section (figure 6(b)) reveals that this droplet is perfectly flat at the top with rather sharp edges. The height of the droplet is approximately 3.7 nm, which is the expected value for four monolayers of OMCTS. The circular droplet moves towards the edge of the contact area within the following 5–10 s, as indicated by the arrow in the inset of figure 6(b).

All these phenomena can be understood qualitatively, if we take into account the elasticity of the substrates. Let us consider the nucleation first. If the two substrates approach at high velocity, the viscosity of the liquid opposes the drainage of the liquid. This leads to an additional

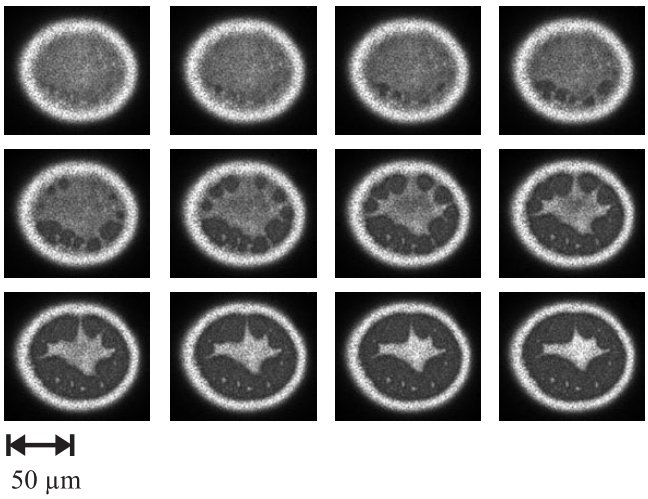

Figure 5. The snapshots are taken from a SFA experiment with thin mica substrates at a high approach rate. The time difference between the images is 0.15 s. Due to the chosen wavelength larger liquid film thickness appears brighter.

pressure that the liquid exerts on the substrates. This contribution is maximal in the centre of the contact line and therefore leads to a large scale outward bending of the substrates. This can be seen clearly in figure 6(a), where we plot a cross-section through the first image of figure 5. The separation between the substrates is minimal close to the edge of the contact area. Hence, this is the region of preferred nucleation.

The lateral shrinkage and the simultaneous increase in thickness are also related to the elastic properties of the substrates. Once the central patch is completely isolated form the edge of the contact area its volume is conserved and it will tend to minimize its energy. If we neglect the line energy, which is reasonable for droplets of several micrometres in diameter, we can approximate the energy by [4]

$$U(\rho, h) = 2p_0\pi\rho^2 + \frac{E}{2(1-\nu^2)}\rho h^2. \tag{4}$$

The first term on the right-hand side is the same as the second one in equation (2). The second one represents the elastic energy required to press a rigid disc of radius ρ and height h by $h/2$ into two semi-infinite elastic substrates on each side [24]. In order to minimize this energy, it may be favourable for the liquid patch to save interfacial energy (first term) by shrinking laterally at the expense of elastic energy (second term). The equilibrium values of ρ and h depend on the amount of trapped material and agree reasonably well with the results from equation (5) [4, 5]. The use of a rigid cylinder approximation in equation (5) is remarkably good, as becomes obvious from figure 6(b). The observation of a flat top is not too surprising, if we take into account the structural forces within this molecularly thin liquid droplet. Obviously, they are strong enough to prevent the droplet from assuming spherical cap shape geometry that one would expect for a bulk liquid.

During the shrinkage the patch develops a slightly brighter rim around its edge (second last and last image in the second row of figure 5). This transient phenomenon is related to material conservation and elastic substrate deformation. Similar phenomena were observed in the dewetting of silicone oil films between a hard Si surface and soft polymeric surface [25] or during dewetting of thin polymer films on solid substrates [26].

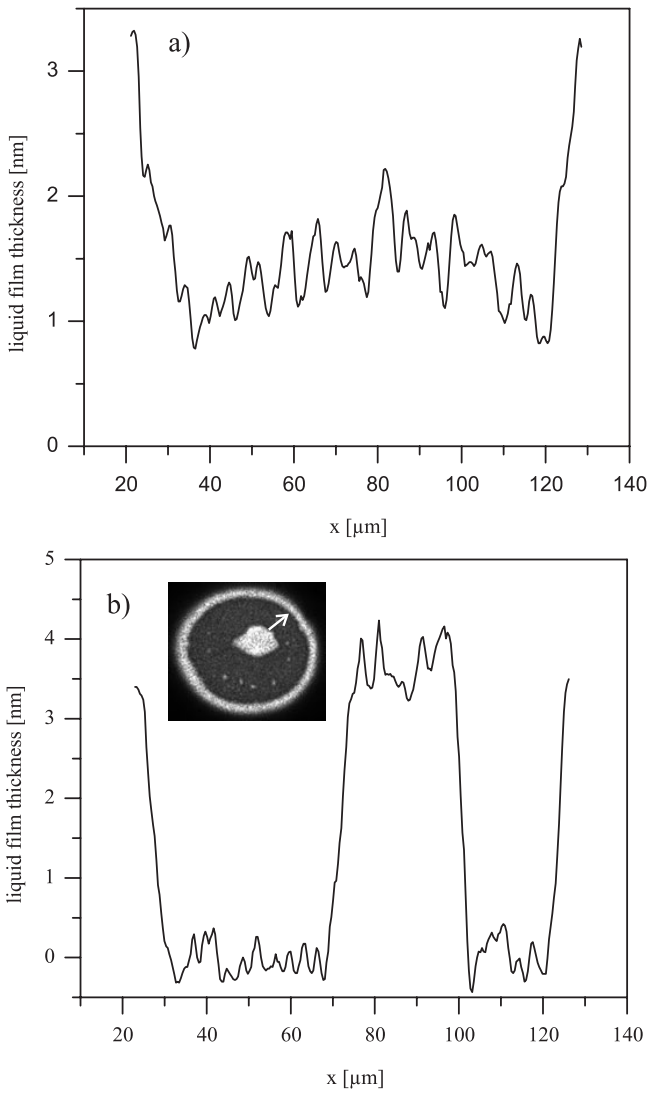

Figure 6. (a) Height profile through the contact area of the first image in figure 5. (b) Cross-section through the contact area with a trapped liquid drop inside. The flat top of the drop indicates a discrete change in film thickness even for trapped amounts of liquids. The calculated thickness of 3.7 ± 0.1 nm is in good agreement with the thickness of four monolayers of OMCTS.

The expulsion of the droplet from the contact zone in the final state is due to the Hertzian pressure distribution. The deformed substrates exert a pressure on the liquid, which is normal to the solid–liquid interface. If integrated over the whole surface of the droplet, this gives rise to a net force. Because of the pressure decrease with increasing ρ according to equation (3), the force is directed along the outward direction. A more detailed analysis of this process, in particular of the flow profile and the dissipation inside the nano-droplet, will be given elsewhere.

5. Summary

Using the two-dimensional imaging capability of our modified SFA, we investigated the dynamics of drainage of molecularly thin liquid films. The spatially resolved imaging technique allows for detailed analysis of hydrodynamic processes in liquid films of nanoscopic thickness. In particular, we showed that the collapse dynamics of lubricant layers in this thickness range depends critically on the elasticity of the substrates.

Acknowledgments

We would like to thank Stephan Herminghaus for interesting discussions. We acknowledge financial support by the German Science Foundation under grant number Mu1472/2-1 within the priority programme 'Wetting and structure formation at interfaces'.

References

[1] Persson B N J 2000 *Sliding Friction—Physical Principles and Applications* (Berlin: Springer)
[2] Israelachvili J N 1991 *Intermolecular and Surface Forces* 2nd edn (London: Academic)
[3] Heuberger M, Zäch M and Spencer N D 2001 *Science* **292** 905
[4] Mugele F and Salmeron M 2000 *Phys. Rev. Lett.* **84** 5796
[5] Mugele F, Becker T, Klingner A and Salmeron M 2002 *Colloids Surf.* A **206** 105
[6] Becker T, Herminghaus S and Mugele F 2002 submitted
[7] Horn R G and Israelachvili J N 1981 *J. Chem. Phys.* **75** 1400
[8] Chan D Y C and Horn R G 1985 *J. Chem. Phys.* **83** 5311
[9] Christenson H K 1983 *J. Chem. Phys.* **78** 6906
[10] Israelachvili J N, McGuiggan P M and Homola A M 1988 *Science* **240** 189
[11] Klein J and Kumacheva E 1995 *Science* **269** 816
[12] Klein J and Kumacheva E 1998 *J. Chem. Phys.* **108** 6996
[13] Demirel A L and Granick S 1996 *Phys. Rev. Lett.* **77** 2261
[14] Demirel A L and Granick S 2001 *J. Chem. Phys.* **115** 1498
[15] Persson B N J and Ballone P 2000 *Solid State Commun.* **115** 599
[16] Persson B N J and Ballone P 2000 *J. Chem. Phys.* **112** 9524
[17] Zilberman S, Persson B N J, Nitzan A, Mugele F and Salmeron M 2001 *Phys. Rev.* E **63** 055103
[18] Persson B N J and Tosatti E 1994 *Phys. Rev.* B **50** 5590
[19] Frantz P and Salmeron M 1998 *Tribol. Lett.* **5** 151
[20] Ohnishi S, Hato M and Christenson H K 1999 *Langmuir* **15** 3312
[21] Born M and Wolf E 1980 *Principles of Optics* (Cambridge, MA: Cambridge University Press)
[22] Curry J E 2001 *Mol. Phys.* **99** 745
[23] Reichert H 2002 *Physik J.* **7/8** 83
[24] Timoshenko S P and Goodier J N 1987 *Theory of Elasticity* (New York: McGraw-Hill) ch 12/138
[25] Martin P and Brochard-Wyart F 1998 *Phys. Rev. Lett.* **80** 3296
[26] Seemann R, Herminghaus S and Jacobs K 2001 *Phys. Rev. Lett.* **87** 196101